

**Experimental and theoretical study of topology and electronic correlations in PuB<sub>4</sub>**

Hongchul Choi, Wei Zhu, S. K. Cary, L. E. Winter, Zhoushen Huang, R. D. McDonald, V. Mocko, B. L. Scott, P. H. Tobash, J. D. Thompson, S. A. Kozimor, E. D. Bauer, Jian-Xin Zhu, and F. Ronning  
*Los Alamos National Laboratory, Los Alamos, New Mexico 87545, USA*

 (Received 18 March 2018; published 29 May 2018)

We synthesize single crystals of PuB<sub>4</sub> using an Al-flux technique. Single-crystal diffraction data provide structural parameters for first-principles density functional theory (DFT) calculations. By computing the density of states, the  $Z_2$  topological invariant using the Wilson loop method, and the surface electronic structure from slab calculations, we find that PuB<sub>4</sub> is a nonmagnetic strong topological insulator with a band gap of 254 meV. Our magnetic susceptibility, heat capacity, and resistivity measurements are consistent with this analysis, albeit with a smaller gap of 35 meV. DFT plus dynamical mean-field theory calculations show that electronic correlations reduce the size of the band gap, and provide better agreement with the value determined by resistivity. These results demonstrate that PuB<sub>4</sub> is a promising actinide material to investigate the interplay of electronic correlations and nontrivial topology.

DOI: [10.1103/PhysRevB.97.201114](https://doi.org/10.1103/PhysRevB.97.201114)

The consequences of nontrivial topologies in materials have attracted widespread interest in recent years [1,2]. Insulators with strong spin-orbit coupling (SOC) can create a band inversion that necessarily leads to the presence of protected surface states. For materials where electronic correlations are weak, first-principles electronic structure approaches have been incredibly powerful in accurately predicting their topology and the corresponding surface states. In the presence of strong electronic correlations, however, new phenomena are anticipated, but are difficult to realize in actual materials [3].  $f$ -electron materials possess both strong spin-orbit coupling and strong electronic correlations and are excellent candidates to explore the combination of nontrivial topologies and correlated electron behavior.

SmB<sub>6</sub> is the most strongly compelling example of a correlated topological insulator, but its small energy scales have resulted in a debate as to the influence of correlations on the proposed surface state [4,5]. Elemental plutonium and its compounds are known to have strong electronic correlations with larger energy scales than their  $4f$  counterparts, and could be helpful in this regard [6,7]. Indeed, PuTe and PuB<sub>6</sub> are predicted to be correlated topological insulators, but lack experimental validation [8,9]. In this Rapid Communication, we have synthesized single crystals of PuB<sub>4</sub>. Our electronic structure calculations indicate this material is also a strong topological insulator, and our transport and thermodynamic measurements support the electronic state proposed by these first-principles calculations. The band gap measured by transport, however, is an order of magnitude smaller than predicted by DFT calculations. Similar to SmB<sub>6</sub>, our DFT plus dynamical mean-field theory (DFT+DMFT) calculations suggest this reflects the presence of electronic correlations. This work demonstrates that PuB<sub>4</sub> is a compelling candidate to investigate the influence of electronic correlations on a topological insulator.

Single crystals of PuB<sub>4</sub> were synthesized with plutonium metal [10] and boron powder using aluminum flux [11]. The crystal structure determined by single-crystal x-ray diffraction

[12,13] and presented in Fig. 1 with  $a = 7.109 \text{ \AA}$  and  $c = 4.009 \text{ \AA}$  is in good agreement with previous work on polycrystalline samples [14–16]. A crystallographically unique Pu atom (shown as blue circles in Fig. 1) is surrounded by three different types of boron atoms, distinguished by red (B1), green (B2), and yellow (B3) circles with Pu-Pu distances longer than typical Pu-Pu bond lengths [17]. From the boron perspective, the solid is best described as having two different boron structure types: B<sub>6</sub>-distorted octahedra (yellow and red) and B<sub>2</sub> linking units (green). Unlike the cubic symmetry of the proposed topological insulators RB<sub>6</sub> ( $R = \text{Sm, Pu}$ ) [18], PuB<sub>4</sub> has tetragonal symmetry, with four formula units (f.u.) in the primitive unit cell. The structure possesses nonsymmorphic symmetries, which impose additional constraints on the electronic structure.

The density of states (DOS) is calculated using density functional theory (DFT) using the generalized gradient approximation as implemented with the WIEN2K code [19,20] (see Supplemental Material [11]). Figures 1(c) and 1(d) demonstrate how the spin-orbit coupling modifies the metallic ground state (blue lines) to an insulating state (red lines). The band gap when including SOC is 254 meV, which is one order of magnitude larger than the tens of meV gaps in RB<sub>6</sub> ( $R = \text{Sm, Pu}$ ) [8,21,22]. Clearly, SOC is essential for establishing the insulating ground state in PuB<sub>4</sub>. Additionally, the near  $E_F$  spectral weight is dominated by Pu  $d$  and Pu  $f$  states, which suggests that electronic correlations may play a role in the physics of PuB<sub>4</sub>.

The electronic band structure including SOC is presented in Fig. 2. At all  $k$  points twofold degeneracies are required by the combined time-reversal and inversion symmetries of the nonmagnetic lattice. The band structure along  $R$ - $A$  and  $M$ - $X$  demonstrates the additional constraint in momentum space forced by the nonsymmorphic symmetry in real space [23]. Along these paths, when  $k_x$  or  $k_y = \pi$ , a fourfold degeneracy occurs. At  $R$ ,  $A$ ,  $M$ , and  $X$ , two different branches merge into one branch to render the fourfold degeneracy.

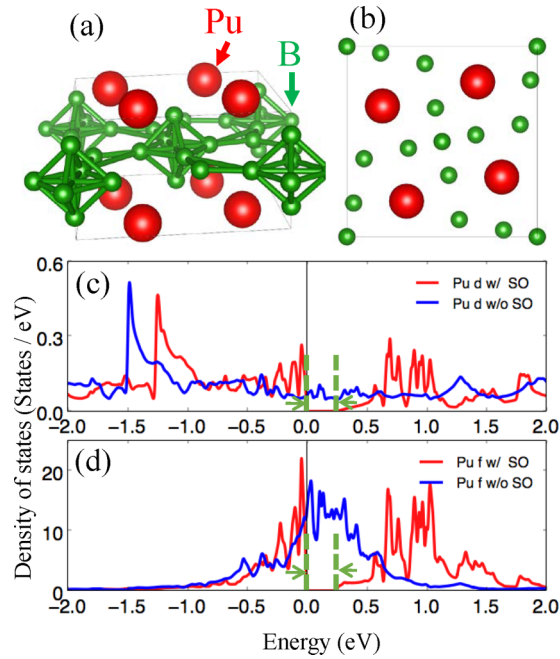


FIG. 1. (a) The crystal structure of  $\text{PuB}_4$ . (b) The top view of the structure shows the nonsymmorphic symmetry, generated by the combined symmetry of mirror and translation symmetries. The local density of states (LDOS) in  $\text{PuB}_4$  with (red) and without (blue) SOC are calculated with the DFT method for (c) the Pu  $d$  and (d) the Pu  $f$  states. The green arrows represent the gap formation with SOC.

To identify the topology of  $\text{PuB}_4$ , we first construct a tight-binding model from the DFT calculation with Pu  $f$ , Pu  $d$ , B  $p$ , and B  $s$  orbitals using the maximally localized Wannier function method (see Refs. [11,24–27]). As shown in Fig. 2, the tight-binding model accurately reproduces the low-energy ( $E_F \pm 2$  eV) electronic structure of  $\text{PuB}_4$ . Using this tight-binding model we investigate the topological property of  $\text{PuB}_4$  by the evolution, or “flow,” of the Wannier centers in momentum space, from which quantized topological indices (the first Chern number or  $Z_2$  number) can then be extracted graphically [28]. Figures 2(b) and 2(c) show the Wilson flow in the  $k_z = 0$  and  $\pi$  planes, respectively. The minimum number of crossings of any horizontal reference line in Figs. 2(b) and 2(c) are 1 and 0, respectively. The three-dimensional  $Z_2$  index is determined by whether the summation of these two numbers is even or odd. The odd number for the Wilson flow asserts that  $\text{PuB}_4$  is a so-called strong topological insulator.

The Wilson flow calculation together with the space group symmetry of the crystal also informs us about the properties of the topologically protected surface states. The single crossing found in Fig. 2(b) means an odd number of exchanges of Kramers partners in the  $k_z = 0$  plane, while there will be an even number of exchanges for  $k_z = \pi$  [Fig. 2(c)]. Since the  $k_z = 0$  plane has effectively two  $X$  points, the exchange occurs at either  $\Gamma$  or  $M$ . The nonsymmorphic symmetry, however, requires a double degeneracy at the  $M$  point, so we can conclude that the exchange must occur at  $\Gamma$ . Therefore, in a slab geometry perpendicular to the  $z$  axis, a topologically protected Dirac cone will emerge on the surface at  $\bar{\Gamma}$  of the surface Brillouin zone.

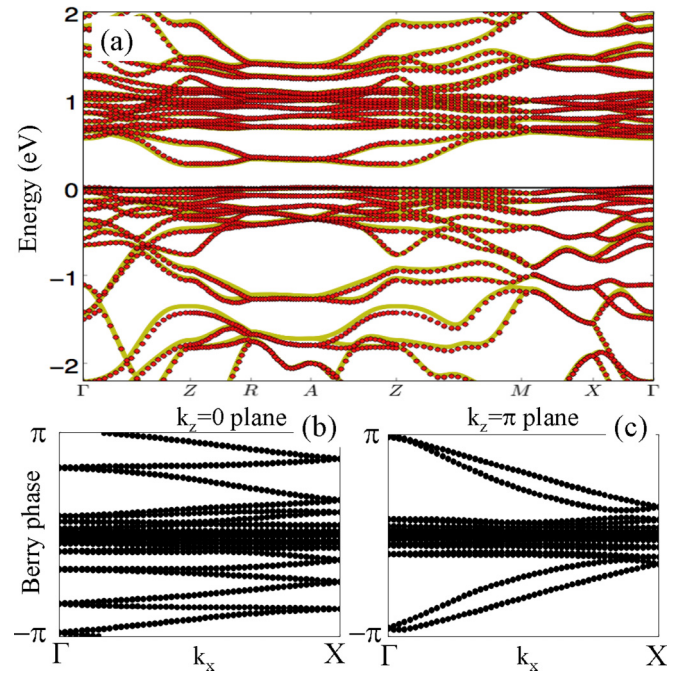


FIG. 2. (a) Comparison of the band structures from the DFT calculation (red circles) with the tight-binding model (yellow line). The black line at 0 eV represents the Fermi level.  $\Gamma$ ,  $Z$ ,  $R$ ,  $A$ ,  $M$ , and  $X$  represent  $(0,0,0)$ ,  $(0,0,\pi)$ ,  $(\pi,0,\pi)$ ,  $(\pi,\pi,\pi)$ ,  $(\pi,\pi,0)$ ,  $(\pi,0,0)$  in reciprocal space. (b), (c) The evolution lines of the Wannier centers for  $\text{PuB}_4$ . The evolution lines cross a horizontal line (b) an odd number of times in the  $k_z = 0$  plane and (c) an even number of times in the  $k_z = \pi$ .

To visualize the topologically protected surface state we computed the electronic structure using a slab geometry. Here,  $1 \times 1 \times 10$  supercells were prepared with and without open boundary conditions at the top and bottom of the supercell. Due to the computational cost, a reduced basis with only Pu  $f$  and Pu  $d$  states was employed to compute the slab geometry. We confirmed that the Wilson loop calculation with the reduced basis set possesses the same topology as in Figs. 2(b) and 2(c). We used the same value of  $E_F$  for the supercells as calculated in the primitive unit cell. Band folding along the  $k_z$  axis results in a complicated and dense band structure. With periodic boundary conditions as in the bulk crystal, the insulating phase is maintained [Fig. 3(a)]. In the presence of open boundary conditions, however, Fig. 3(b) illustrates the Dirac cone arising at  $\Gamma$ , as expected from the Wilson flow calculation. Due to the existence of surfaces at the top and bottom of the slab, the Dirac point realizes a fourfold degeneracy. We note that several trivial surface states also manifest due to the large number of Pu  $f$  and  $d$  orbitals at the surface. Both calculations of the Wilson flow and the surface electronic band structure establish a nontrivial topology of  $\text{PuB}_4$  using a DFT approach.

Validating the DFT calculations, experiments demonstrate that  $\text{PuB}_4$  is a nonmagnetic insulator. Magnetic susceptibility measurements are shown in Fig. 4(a) for a 42.5-mg sample composed of an aggregate of many crystals. The lack of local magnetic moments is reflected by the small and weak temperature dependence of the magnetic susceptibility, in agreement with previous studies and similar to that found in

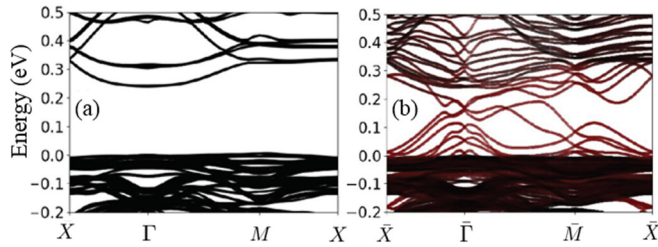


FIG. 3. (a) The  $1 \times 1 \times 10$  supercell band structure and (b) its surface states of  $\text{PuB}_4$  on a (001) surface.  $X, \Gamma, M$  in (a) are  $(\pi, 0, 0), (0, 0, 0), (\pi, \pi, 0)$  in the supercell Brillouin zone, and  $\bar{X}, \bar{\Gamma}, \bar{M}$  in (b) are  $(\pi, 0), (0, 0), (\pi, \pi)$  in the surface Brillouin zone perpendicular to the  $z$  axis. Red bands emphasize surface derived states.

other paramagnetic insulators [29]. The small positive value may be a result of a Van Vleck contribution or from in-gap states. At low temperatures there is a small increase most likely originating from a minor magnetic impurity of unknown origin. Heat capacity measurements in Fig. 4(b) reveal a tiny residual electronic term. We fit the specific heat to the expression  $C/T = \gamma + \beta T^2$  below 11 K. This yields  $\gamma = 2.5 \text{ mJ/mol K}^2$  and a Debye temperature  $\theta_D = 430 \text{ K}$  from the formula  $\theta_D = [12 \pi^4 n R / (5\beta)]^{1/3}$ , where  $R$  is the gas constant and  $n = 5$  for the number atoms per formula unit. The residual  $\gamma$  term is much smaller than what is found in  $\text{SmB}_6$  [30,31], which we believe reflects localized in-gap states of unknown origin. A large Wilson ratio  $R_W \sim 11$  in this nonmagnetic compound implies that the susceptibility and linear specific heat coefficient have different origins.

The insulating nature of  $\text{PuB}_4$  is confirmed by the resistivity measurements shown in Fig. 5. At temperatures below roughly 100 K, the resistivity rolls over and begins to saturate. Presently, it is impossible to determine whether the resistivity

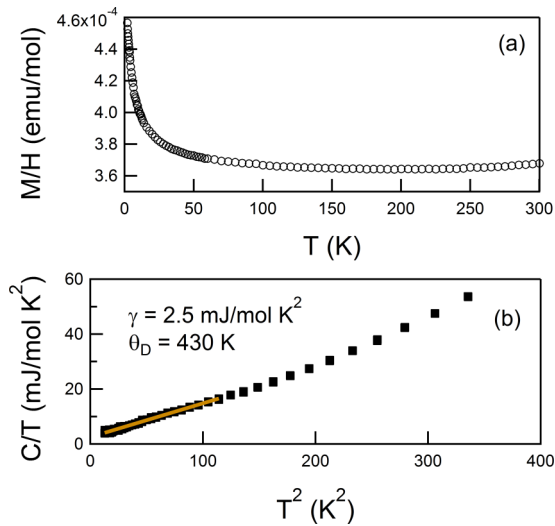


FIG. 4. (a) Magnetization ( $\Delta M$ ) at 5 T divided by the magnetic field vs the temperature. (b) Low-temperature specific heat divided by temperature vs the square of the temperature. The solid line is a linear fit to the data, whose  $y$  intercept provides the electronic contribution characterized by  $\gamma$ , while the slope provides the phonon contribution characterized by  $\theta_D$ .

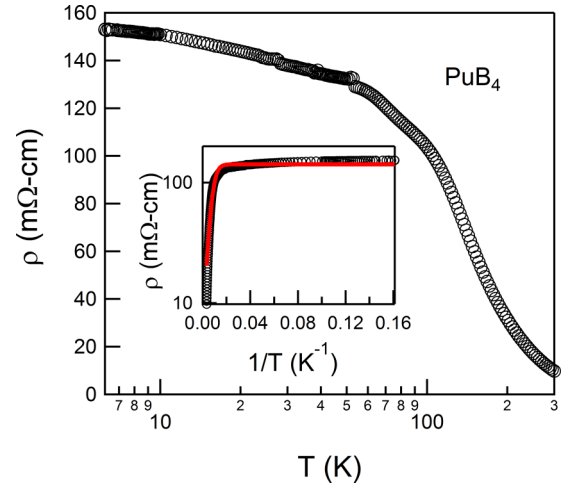


FIG. 5. Resistivity of a  $\text{PuB}_4$  single crystals vs temperature. The inset shows a plot vs inverse temperature, where the solid red line is a fit to a two-channel model yielding a bulk gap of 35 meV as described in the text.

saturation is a consequence of in-gap states as observed in many  $\text{Bi}_2\text{Se}_3$  samples [32] or from a metallic surface state as observed in  $\text{SmB}_6$  and some high-quality  $\text{Bi}_2\text{Se}_3$  thin films [33–35]. We were unable to vary the thickness sufficiently systematically to draw a conclusion regarding this point. As shown in the inset of Fig. 5, we fit the resistivity to a parallel conduction model  $\rho = \{1/\rho_0 + 1/[\rho_b \exp(\Delta/k_B T)]\}^{-1}$  with one channel corresponding to a temperature-independent metallic channel that would arise from a surface or impurity band and a second channel corresponding to the activated bulk behavior. This fit gives  $\Delta = 35 \text{ meV}$  for the bulk behavior, which is significantly smaller than the band gap determined by DFT. The resistivity at the lowest temperatures does not saturate as quickly as the simple two-channel model would indicate. This may reflect some degree of localization or other correlation effect on the low-temperature transport, which requires further investigation.

These calculations and measurements on  $\text{PuB}_4$  show that it has properties similar to those of  $\text{SmB}_6$ , but with an order of magnitude larger energy scale in the tetraboride (see Table I). In  $\text{SmB}_6$ , the DFT determined band gap is  $\approx 15 \text{ meV}$  [21,22], which is larger than the gap of  $\approx 2.3 \text{ meV}$  measured by resistivity [36]. Below  $T^* \approx 4 \text{ K}$  there is a crossover in  $\text{SmB}_6$  to a metallic surface dominated regime [33,37]. In  $\text{PuB}_4$ , both the DFT and resistively determined gaps are roughly an order

TABLE I. Comparison of several properties of  $\text{PuB}_4$  vs  $\text{SmB}_6$ . Values for  $\text{PuB}_4$  are from this work, while values for  $\text{SmB}_6$  come from the references given in the last column.

	$\text{PuB}_4$	$\text{SmB}_6$	Refs.
$\Delta_{\text{DFT}}$ (meV)	254	14–23	[21,22]
$\Delta_\rho$ (meV)	35	2.3	[36]
$T^*$ (K)	100	4	[33,37]
$\chi_o$ (emu/mol)	$3.6 \times 10^{-4}$	$3 \times 10^{-3}$	[36]
$\gamma_{\text{resid}}$ (mJ/mol K <sup>2</sup> )	2.5	7–30	[30,31]

TABLE II. Variation of the gap between valence and conduction bands as a function of  $U$  (on-site Coulomb interaction).

$U$ (eV)	Correlation effect on the gap size				Experiment
	0	3.5	4.0	4.5	
Gap size (meV)	253.6	15.2	13.2	10.3	35

of magnitude larger than in  $\text{SmB}_6$ , and the crossover to a resistively saturating regime occurs roughly 25 times higher in temperature. Additionally, the magnetic susceptibility and residual specific heat values are both roughly an order of magnitude smaller in  $\text{PuB}_4$  relative to  $\text{SmB}_6$ , as one might expect if the energy scales are an order of magnitude larger. This comparison suggests that  $\text{PuB}_4$  is an analog of  $\text{SmB}_6$  with larger energy scales, which may ease interrogation of its surface states with angle-resolved photoemission spectroscopy (ARPES) and/or scanning tunneling microscopy (STM).

In  $\text{SmB}_6$ , strong electronic correlations renormalize the DFT determined band gap from  $\approx 15$  meV to the experimentally measured gap of  $\approx 2.3$  meV without changing the topology of the system [38–40]. To see if correlations play a similar role in  $\text{PuB}_4$ , we investigate the gap size using DFT+DMFT, where an on-site Coulomb interaction ( $U$ ) is added to the  $f$  electron [11,41,42]. Table II shows the theoretically determined gap size as a function of  $U$ . The value at  $U = 0.0$  eV corresponds to the gap calculated by DFT, shown in Fig. 1. Since we use the strong-coupling-based impurity solver, we could not describe the states near the DFT ground state with negligible  $U$ . Typical  $U$  values for Pu are 4–4.5 eV [6,43–45], and in that range self-consistency could be achieved. As a function of  $U$  from 3.5 to 4.5 eV, the computed band gaps decrease from 15.2 to 10.3 meV. By including the effects of correlations on the Pu  $5f$  electrons, the DFT+DMFT band gap is reduced by one order of magnitude relative to the overestimated DFT band gap, which supports the notion

that electronic correlations play an important role in  $\text{PuB}_4$ . Furthermore, we note that a spin-polarized DFT calculation without  $U$  incorrectly predicts a magnetic ground state in contradiction with the experimental results, thereby necessitating the need to include correlations. Because the insulating phase is maintained throughout the DFT+DMFT calculations, the robustness of the nontrivial topology is presumed.

In summary, transport and thermodynamic measurements on single crystals of  $\text{PuB}_4$  demonstrate that it is a nonmagnetic insulator. This is consistent with DFT calculations, which suggest that  $\text{PuB}_4$  is a strong topological insulator. This may explain the saturating resistivity behavior at low temperatures. The presence of electronic correlations is revealed by the renormalization of the band gap as measured by resistivity, and reproduced in our DFT+DMFT calculations. Experimentally,  $\text{PuB}_4$  shares many similarities with  $\text{SmB}_6$ , but with a larger energy scale. Our results suggest that  $\text{PuB}_4$  is a promising candidate to explore the effect of electronic correlations in a topologically nontrivial material. Spectroscopic probes, such as ARPES and STM, will be particularly valuable to understand this interplay.

We immensely appreciate Zach Fisk and Priscila Rosa for assistance with the crystal growth and gratefully acknowledge the Los Alamos National Laboratory Laboratory Directed Research and Development (LDRD-DR 20160085DR) for support (J.C., W.Z., L.E.W., Z.H., R.D.McD., P.H.T., J.D.T., S.A.K., E.D.B., J.-X.Z., F.R.). Portions of this work were also supported by the LDRD office through a Darleane Christian Hoffman Distinguished Postdoctoral Fellowship (S.K.C.). We also acknowledge support through the LANL Heavy Element Chemistry Program that is funded by the Division of Chemical Sciences, Geosciences, and Biosciences, Office of Basic Energy Sciences, U.S. Department of Energy (V.M., B.L.S.). Los Alamos National Laboratory is operated by Los Alamos National Security, LLC, for the National Nuclear Security Administration of U.S. Department of Energy (Contract No. DE-AC52-06NA25396).

- 
- [1] M. Z. Hasan and C. L. Kane, *Rev. Mod. Phys.* **82**, 3045 (2010).
- [2] X.-L. Qi and S.-C. Zhang, *Rev. Mod. Phys.* **83**, 1057 (2011).
- [3] For example, see A. Stern, *Annu. Rev. Condens. Matter Phys.* **7**, 349 (2016).
- [4] M. Dzero, K. Sun, V. Galitski, and P. Coleman, *Phys. Rev. Lett.* **104**, 106408 (2010).
- [5] M. Dzero, J. Xia, V. Galitski, and P. Coleman, *Annu. Rev. Condens. Matter Phys.* **7**, 249 (2016).
- [6] J. H. Shim, K. Haule, and G. Kotliar, *Nature (London)* **446**, 513 (2007).
- [7] C. H. Booth, Y. Jiang, D. L. Wang, J. N. Mitchell, P. H. Tobash, E. D. Bauer, M. A. Wall, P. G. Allen, D. Sokaras, D. Nordlund, T.-C. Weng, M. A. Torrez, and J. L. Sarrao, *Proc. Natl. Acad. Sci. USA* **109**, 10205 (2012).
- [8] X. Deng, K. Haule, and G. Kotliar, *Phys. Rev. Lett.* **111**, 176404 (2013).
- [9] X. Zhang, H. Zhang, J. Wang, C. Felser, and S.-C. Zhang, *Science* **335**, 1464 (2012).
- [10] National Nuclear Data Center, Brookhaven National Laboratory, <http://www.nndc.bnl.gov/chart/> (6 February 2018).
- [11] See Supplemental Material at <http://link.aps.org/supplemental/10.1103/PhysRevB.97.201114> for details on the synthesis and crystallographic structure, as well as the methods used for the electronic structure calculations.
- [12] S. K. Cary, K. S. Boland, J. N. Cross, S. A. Kozimor, and B. L. Scott, *Polyhedron* **126**, 220 (2017).
- [13] A. Spek, *J. Appl. Crystallogr.* **36**, 7 (2003).
- [14] B. J. McDonald and W. I. Stuart, *Acta Crystallogr.* **13**, 447 (1960).
- [15] H. A. Eick, *Inorg. Chem.* **4**, 1237 (1965).
- [16] P. Rogl and P. Potter, *J. Phase Equilib.* **18**, 467 (1997).
- [17] F. J. Espinosa, P. Villela, J. C. Lashley, S. D. Conradson, L. E. Cox, R. Martinez, B. Martinez, L. Morales, J. Terry, and R. A. Pereyra, *Phys. Rev. B* **63**, 174111 (2001).
- [18] Z. Fisk, P. H. Schmidt, and L. D. Longinotti, *Mater. Res. Bull.* **11**, 1019 (1976).

- [19] P. Blaha, K. Schwarz, G. Madsen, D. Kvasicka, and J. Luitz, *WIEN2K, An Augmented Plane Wave + Local Orbitals Program for Calculating Crystal Properties* (Technical University of Vienna, Vienna, 2001).
- [20] J. P. Perdew, K. Burke, and M. Ernzerhof, *Phys. Rev. Lett.* **77**, 3865 (1996).
- [21] A. Yanase and H. Harima, *Prog. Theor. Phys. Suppl.* **108**, 19 (1992).
- [22] V. N. Antonov, B. N. Harmon, and A. N. Yaresko, *Phys. Rev. B* **66**, 165209 (2002).
- [23] S. M. Young and C. L. Kane, *Phys. Rev. Lett.* **115**, 126803 (2015).
- [24] J. Kunes, R. Arita, P. Wissgott, A. Toschi, H. Ikeda, and K. Held, *Comput. Phys. Commun.* **181**, 1888 (2010).
- [25] N. Marzari and D. Vanderbilt, *Phys. Rev. B* **56**, 12847 (1997).
- [26] I. Souza, N. Marzari, and D. Vanderbilt, *Phys. Rev. B* **65**, 035109 (2001).
- [27] A. A. Mostofi, J. R. Yates, G. Pizzi, Y. S. Lee, I. Souza, D. Vanderbilt, and N. Marzari, *Comput. Phys. Commun.* **185**, 2309 (2014).
- [28] R. Yu, X. L. Qi, A. Bernevig, Z. Fang, and X. Dai, *Phys. Rev. B* **84**, 075119 (2011).
- [29] J. L. Smith and H. H. Hill, Magnetism in neptunium borides, in *Magnetism and Magnetic Materials-1974: 20th Annual Conference, San Francisco*, edited by C. D. Graham, Jr., G. H. Lander, and J. J. Rhyne, AIP Conf. Proc. Vol. 24 (AIP, New York, 1975), p. 382.
- [30] T. Kasuya, K. Takegahara, T. Fujita, T. Tanaka, and E. Bannai, *J. Phys. (Paris)* **40**, C5-308 (1979).
- [31] W. A. Phelan, S. M. Koochpayeh, P. Cottingham, J. W. Freeland, J. C. Leiner, C. L. Broholm, and T. M. McQueen, *Phys. Rev. X* **4**, 031012 (2014).
- [32] S. Barua and K. P. Rajeev, *AIP Adv.* **4**, 017135 (2014).
- [33] D. Kim, S. Thomas, T. Grant, J. Botimer, Z. Fisk, and J. Xia, *Sci. Rep.* **3**, 3150 (2013).
- [34] D. J. Kim, J. Xia, and Z. Fisk, *Nat. Mater.* **13**, 466 (2014).
- [35] A. A. Taskin, S. Sasaki, K. Segawa, and Y. Ando, *Phys. Rev. Lett.* **109**, 066803 (2012); N. Bansal, Y. S. Kim, M. Brahlek, E. Edrey, and S. Oh, *ibid.* **109**, 116804 (2012).
- [36] A. Menth, E. Buehler, and T. H. Geballe, *Phys. Rev. Lett.* **22**, 295 (1969).
- [37] J. W. Allen, B. Batlogg, and P. Wachter, *Phys. Rev. B* **20**, 4807 (1979).
- [38] T. Takimoto, *J. Phys. Soc. Jpn.* **80**, 123710 (2011).
- [39] F. Lu, J. Z. Zhao, H. Weng, Z. Fang, and X. Dai, *Phys. Rev. Lett.* **110**, 096401 (2013).
- [40] J. Kim, K. Kim, C.-J. Kang, S. Kim, H. C. Choi, J.-S. Kang, J. D. Denlinger, and B. I. Min, *Phys. Rev. B* **90**, 075131 (2014).
- [41] G. Kotliar, S. Y. Savrasov, K. Haule, V. S. Oudovenko, O. Parcollet, and C. A. Marianetti, *Rev. Mod. Phys.* **78**, 865 (2006).
- [42] K. Haule, C.-H. Yee, and K. Kim, *Phys. Rev. B* **81**, 195107 (2010).
- [43] M.-T. Suzuki and P. M. Oppeneer, *Phys. Rev. B* **80**, 161103(R) (2009).
- [44] J.-X. Zhu, P. H. Tobash, E. D. Bauer, F. Ronning, B. L. Scott, K. Haule, G. Kotliar, R. C. Albers, and J. M. Wills, *Europhys. Lett.* **97**, 57001 (2012).
- [45] J.-X. Zhu, R. C. Albers, K. Haule, G. Kotliar, and J. M. Wills, *Nat. Commun.* **4**, 2644 (2013).